TABLE I. Oligonucleotide Primer Sequences in Real-Time RT-PCR

Target cDNA		Primer Sequence (5′-3′)	T_m (°C)	Length (bp)	GenBank Accession Numbers
Coll	F	TGCTGGACGTCCTGGTGAAG	64.8	20	NM 007742
	R	ACGTTGTCCAGCAATACCCTGAG	64.6	23	
OPN	F	TACGACCATGAGATTGGCAGTGA	65.0	23	NM 009263
	R	TATAGGATCTGGGTGCAGGCTGTAA	65.0	25	
GAPDH	F	TGTGTCCGTCGTGGATCTGA	63.8	20	NM 001001303
	R	TTGCTGTTGAAGTCGCAGGAG	63.9	21	

Giemsa's staining. For Giemsa's staining, the medium was aspirated from the wells, and the cells were rinsed with a PBS(−) solution. The cells were fixed with 4% formalin. Then, the cells were rinsed with ultrapure water. They were then stained with a 10% Giemsa's solution (Merck KGaA) at room temperature for 15 min. The cells were repeatedly rinsed with ultrapure water after immersion in the Giemsa's solution. On the other hand, the cells on the sputter-deposited Ti and PS dish were observed using a phase-contrast microscope without any treatments.

In addition, MC3T3-E1 cells cultured for 3 days on each specimen were retrieved by trypsinization. They were counted on a hematocytometer with the trypan blue staining. Three specimens were used under the same experimental condition. The data were analyzed by the Student's two-tailed *t*-test.

Alkaline phosphatase activity staining

Alkaline phosphatase (ALP) activity of the MC3T3-E1 cells differentiation-induced on each specimen was evaluated by staining after 0, 3, 5, 7, 10, 14, and 21 days from differentiation induction. The medium was aspirated from the wells, and the cells were rinsed with a PBS(−) solution before staining. The cells were fixed with 4% formalin and then rinsed with ultrapure water. After fixation, the cells on each specimen were stained using an AP Conjugate Substrate Kit (Bio-Rad Laboratories, Hercules, CA) following standard procedures. Three specimens were used under the same experimental condition for all differentiation terms.

Gene expression analysis

The total RNA of MC3T3-E1 cells differentiation-induced for 10 days on each specimen was isolated using a TRIzol®

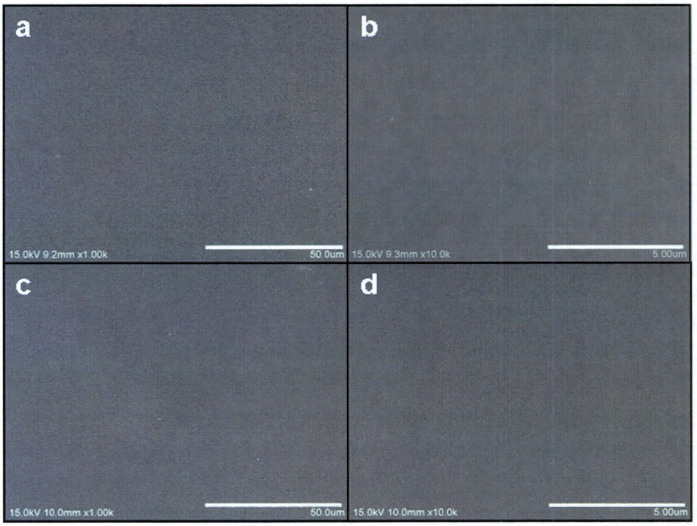

FIGURE 1. Scanning electron micrographs of (a, b) mirror-polished bulk and (c, d) sputter-deposited Ti specimens. The sputter deposition was carried out on the cover glasses. Higher-magnification pictures of (a, c): Scale bar: 50 μm; and lower-magnification pictures of (b, d): Scale bar: 5 μm.

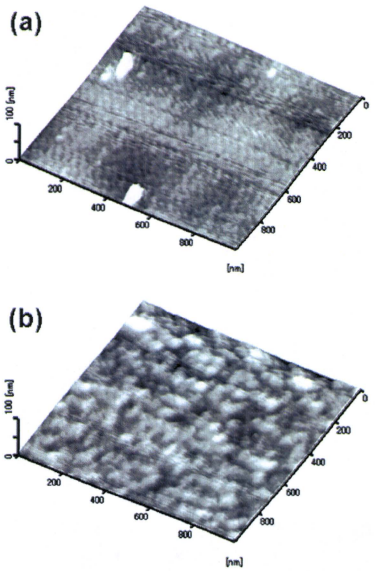

FIGURE 2. Scanning probe micrographs of (a) mirror-polished bulk and (b) sputter-deposited Ti specimens. The sputter deposition was carried out on the cover glasses.

reagent (Invitrogen, Carlsbad, CA) following standard procedures. For real-time PCR analysis, total RNA was reverse-transcribed with a PrimeScript™ RT reagent kit (Takara Bio, Shiga, Japan) following standard procedures. Synthesized cDNA was amplified by real-time PCR on an ABI 7300 Prism real-time PCR instrument (Applied Biosystems, Foster City, CA) using SYBR® *Premix Ex Taq*™ (Takara Bio) following standard procedures. Primers for PCR were Type I collagen (Coll), osteopontin (OPN), and glyceraldehyde-3-phosphate dehydrogenase (GAPDH) (Table I). The housekeeping gene of GAPDH was used as an internal control in the reactions. This analysis was carried out using the total RNA extracted from cells differentiation-induced on one specimen under the same condition and repeated three times. The obtained data were analyzed by the comparative Ct method ($2^{-\Delta\Delta C_t}$ method).[3] The data were analyzed by the Student's two-tailed *t*-test.

RESULTS

Surface observation

The scanning electron micrographs and scanning probe micrographs of the surfaces on the bulk and sputter-deposited Ti are shown in Figures 1 and 2. In addition, the parameters of surface roughness determined with SPM image data, i.e., the values of R_a, R_y, R_q, and S ratio, were summarized in Table II. The surface was randomly observed on each specimen. From the SEM and SPM images, the surfaces of both specimens were sufficiently smooth. In addition, there was no significant difference in the surface roughness on each specimen. However, the standard deviation (SD) of the R_a, R_y, and R_q values on the sputter-deposited Ti were significantly smaller than those on the bulk Ti. The surface on the sputter-deposited Ti was more uniform than that on the bulk Ti, while both surfaces were smooth.

Surface characterization

XPS spectra of binding energy regions of Ti 2p, O 1s, N 1s, and C 1s were obtained from both specimens. Contaminant carbon is detected from XPS as usual. Therefore, no extra contamination was detected in this study. The XPS spectra of Ti 2p and O 1s regions of the bulk and sputter-deposited Ti were shown in Figure 3. The Ti 2p spectra of both the bulk and sputter-deposited Ti gave four peaks according to valence, Ti^0, Ti^{2+}, Ti^{3+}, and Ti^{4+}; the O 1s spectra of both specimens gave three peaks, O^{2-}, OH^-, and H_2O.[4,5] The fractional parts of each element were summerelized in Tables III and IV. Titanium existed as metallic and oxide states in a detectable depth with XPS. Therefore, the surface oxide films on both specimens were very thin because the metallic states, Ti^0, were detected through the surface oxide films. In addition, the thickness of oxide film on the sputter-deposited Ti was smaller than that on the bulk Ti because the proportion of the integrated intensity of Ti^0 on the sputter-deposited Ti was larger than that on the bulk Ti. On the other hand, the surface oxide film on each specimen mainly consisted of TiO_2 with small amounts of TiO and Ti_2O_3. The oxide films contained hydroxide, hydroxyl groups, and water. However, the proportions of TiO and Ti_2O_3 in the surface oxide film on the sputter-deposited Ti were larger than those on the bulk Ti, because the proportions of the integrated intensities of Ti^{2+} and Ti^{3+} on the sputter-deposited Ti were larger than those on the bulk Ti.

Cell attachment and number

The morphology of cells cultured on each specimen for 3 days after seeding is shown in Figure 4. The cells were adhered and extended well on each specimen. No significant difference in cell attachment status and morphology was observed.

TABLE II. Roughness Parameters of Bulk and Sputter-deposited Titanium Surfaces

	R_a (nm)	R_y (nm)	R_q (nm)	S ratio
Bulk Ti	1.853 ± 0.873	28.01 ± 10.63	2.561 ± 1.119	1.011 ± 0.004
Sputter-deposited Ti	1.347 ± 0.026	13.69 ± 0.84	1.711 ± 0.034	1.018 ± 0.009

The data are the mean ± SD; $n = 3$.

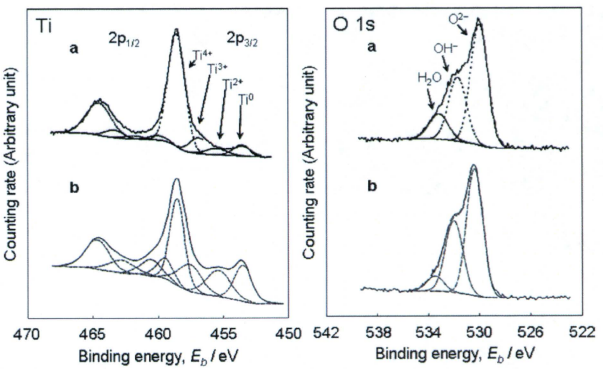

FIGURE 3. XPS spectra of Ti 2p and O 1s regions obtained from (a) bulk Ti and (b) sputter-deposited Ti and their component peaks.

The number of cells cultured on each specimen for 3 days after seeding is shown in Figure 5. There was no significant difference in the cell numbers among all specimens. In this study, the living cells were counted on the hematocytometer with trypan blue staining. The trypan blue solution stains the dead cells but not the living ones. There were few dead cells, indicating that not all specimens showed cytotoxicity. It is well known that titanium is safe for use as a biomedical material.

ALP activity

The time transient pictures by ALP activity staining on each specimen are shown in Figure 6. In this staining, the ALP-positive cells were stained. The ALP activities increased in all specimens from the beginning of differentiation induction. It is known that the ALP activity of MC3T3-E1 cells increases after differentiation induction, then decreases once at the beginning of cell mineralization, and then increases once again.[6] In addition, it is demonstrated that the ALP activity did not directly concern with the osteoblast calcification.[7] Therefore, the time of the maximum activity differentiation-induced on each specimen was focused in this study. The time showing maximum ALP activity on the bulk Ti and PS dish seemed to be recorded at around 10 days. On the other hand, the time on the sputter-deposited Ti seemed to be retarded, being recorded at around 14 days. Therefore, it was suggested that the ALP activity on the bulk Ti was superior to that on the sputter-deposited Ti.

TABLE III. Fractional Parts of Ti^0, Ti^{2+}, Ti^{3+}, and Ti^{4+} on Bulk and Sputter-deposited Titanium Surfaces

	Ti^0	Ti^{2+}	Ti^{3+}	Ti^{4+}
Bulk Ti	0.07	0.05	0.12	0.76
sputter-deposited Ti	0.21	0.20	0.19	0.40

Gene expression analysis by real-time RT-PCR

The expression levels of Coll and OPN genes differentiation-induced on each specimen for 10 days are shown in Figures 7 and 8, respectively. All data were normalized to GAPDH housekeeping gene. The relative strength of Coll mRNA on each specimen was as follows: Bulk Ti; 0.590 ± 0.150, sputter-deposited Ti; 0.942 ± 0.124, and PS dish; 0.801 ± 0.076. The relative strength of OPN mRNA on each specimen was as follows: Bulk Ti; 1.754 ± 0.241, sputter-deposited Ti; 1.121 ± 0.203, and PS dish; 1.400 ± 0.158. The expression level of Coll on the sputter-deposited Ti was higher than that on the bulk Ti. The bone matrix consists mainly of Coll, which is secreted by osteoblasts and is assembled in the matrix macromolecular structures that give tensile strength and act as a scaffold for mineralization. Coll increases during the early stages of differentiation.[8–11] On the other hand, the expression level of OPN on the bulk Ti was significantly higher than that on the sputter-deposited Ti. OPN is a phosphoprotein which is found in the bone extracellular matrix.[12–14] This marker is upregulated later than Coll in osteoblast differentiation.[8–11] These results indicate that bone differentiation was faster on the bulk Ti than on the sputter-deposited Ti.

DISCUSSION

In this study, all specimens were autoclaved with RO water and the autoclave apparatus whose chamber was carefully

TABLE IV. Fractional Parts of O^{2-}, OH^-, and H_2O on Bulk and Sputter-deposited Titanium Surfaces

	O^{2-}	OH^-	H_2O
Bulk Ti	0.57	0.30	0.13
Sputter-deposited Ti	0.59	0.35	0.06

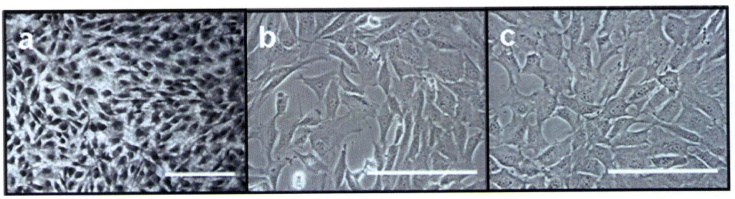

FIGURE 4. MC3T3-E1 cell morphologies cultured for 3 days on (a) mirror-polished bulk Ti, (b) sputter-deposited Ti, and (c) PS dish. The cells on (a) were stained with Giemsa's solution, and the cells on (b, c) did not undergo any treatments. Optical micrograph of (a) and phase-contrast micrographs of (b, c). Scale bar: 200 μm.

cleaned with ethanol. It was demonstrated that no contamination was added to titanium surface by the same autoclaving process as this study.[15] Therefore, the autoclaving process did not affect to the differentiation of osteoblastic cells.

From the ALP activity staining and gene expression analysis, the osteogenesis in MC3T3-E1 cells differentiation-induced on the bulk Ti was faster than that on the sputter-deposited Ti. As described in the "Introduction" section, the bulk Ti has a crystal structure, but the sputter-deposited Ti has an amorphous structure. Titanium is passivated by forming a thin oxide film on its surface. Defects reflected by the composition of titanium, such as grain boundaries and compositional segregations, exist in the surface oxide film on the bulk Ti. On the other hand, the oxide film on the sputter-deposited Ti is more uniform than that on the bulk Ti because it does not present any grain boundaries. Therefore, the condition of the surface oxide film is different between the bulk and sputter-deposited Ti. This difference may affect the bone differentiation properties of osteogenic cells: The cells adhered on each specimen may undergo different effects from each surface.

From the XPS analysis, the thickness of surface oxide film on the sputter-deposited Ti was smaller than that on the bulk Ti. In addition, the compositions of surface oxide films on the bulk and sputter-deposited Ti were different each other: The proportions of TiO and Ti_2O_3 in the surface oxide film on sputter-deposited Ti were larger than those on the bulk Ti. Cellular function is influenced by the conformational changes of proteins adsorbed on the material surfaces. The electrostatic force of a solid material influences the change in the conformation of the proteins adsorbed on the material.[16] The electrostatic force is determined by the relative permittivity of the surface oxide film. The relative permittivity of TiO_2 (86–170) is similar to that of H_2O (80.1).[17] On the other hand, that of Ti_2O_3 is 30 that is much smaller than the aforementioned values. The surface oxide film on the bulk Ti consist of mainly TiO_2 containing small amount of TiO and Ti_2O_3, while that on the sputter-deposited Ti contains large amounts of TiO and Ti_2O_3. Therefore, the electrostatic force of the bulk Ti is smaller than that of the sputter-deposited Ti; the conformational changes of proteins adsorbed on the bulk Ti is smaller than that on the sputter-deposited Ti. This difference may influence that the differentiation properties of MC3T3-E1 cells on the bulk Ti was superior to those on the sputter-deposited Ti.

From the SEM and SPM observations, the surfaces on both the bulk and sputter-deposited Ti were smooth (Figs. 1 and 2). In addition, there were no significant differences in any roughness parameters between the bulk and sputter-deposited Ti. However, the SD of the R_a, R_y, and R_q values on the bulk Ti were much larger than those on the sputter-deposited Ti. The sputter-deposited Ti was prepared by the sputter deposition technique, and titanium was physically adsorbed on the smooth cover glasses at an atomic level; on the other hand, the bulk Ti was prepared by mirror-polishing using abrasives, and the surface was physically polished. Therefore, some asperities at the nanometer level, attributed to the polishing, were

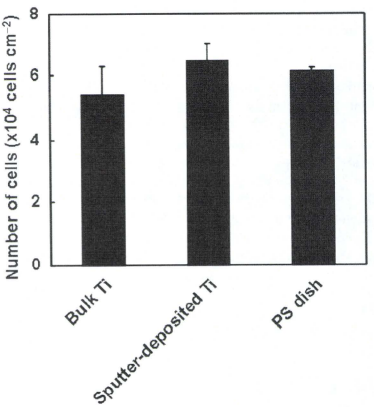

FIGURE 5. Number of MC3T3-E1 cells cultured for 3 days on mirror-polished bulk Ti, sputter-deposited Ti, and PS dish. Cells were counted using a hematocytometer with trypan blue staining after trypsinization. The data are the mean ± SD; $n = 3$. There was no significant difference among all specimens; $p > 0.05$.

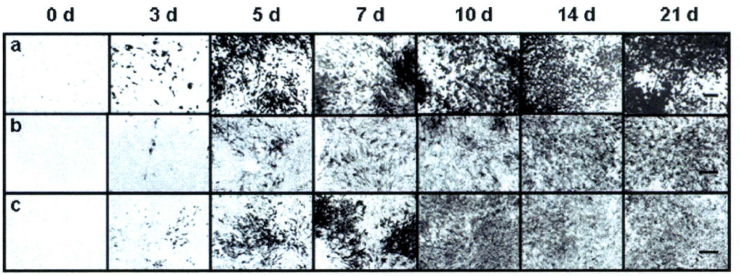

FIGURE 6. Time course of ALP activity stained MC3T3-E1 cells on (a) mirror-polished bulk Ti, (b) sputter-deposited Ti, and (c) PS dish. The ALP-positive cells were stained. Optical micrographs of (a) and phase-contrast micrographs of (b, c). Scale bar: 400 μm.

present on the bulk Ti. Furthermore, some impurities, such as abrasives, were also present on it. From the SPM image of the bulk Ti, some projections in the scale of a few dozen nanometers were observed. These impurities may have been the result of polishing. Although the bulk Ti was sufficiently rinsed by ultrasonication in acetone, it was difficult to completely remove all contaminants from the surface. Therefore, the surface roughness on the bulk Ti was partially large at the nanometer level because of some asperities and abrasives, while the surface on the sputter-deposited Ti was sufficiently smooth and clean. It is well known that the titanium surface condition and roughness affect the osteoblastic behavior. The number of human osteoblastic cells that proliferated on the smooth titanium was lower than that on the rough titanium. In addition, the expression of ALP, prostaglandin E_2, and TGF-β on the rough titanium was comparatively higher than that on the smooth titanium *in vitro*.[18,19] Coll and osteocalcin expression were also enhanced.[20] Furthermore, the osteoblast adhesion increased on nanophase titanium, Ti-6Al-4V, and Co-Cr-Mo.[21] However, no significant differences were observed in the proliferative rates of osteoblasts cultured on sandblasted and grooved (600 grit) commercially pure titanium and the tissue-culture-treated

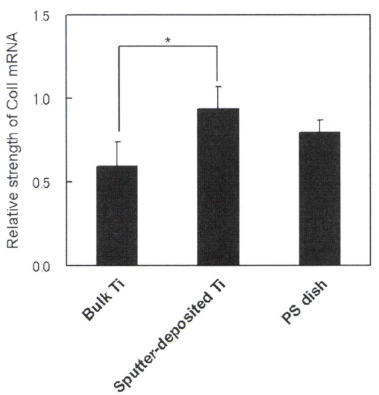

FIGURE 7. Coll gene expression analysis of MC3T3-E1 cells differentiation-induced for 10 days on mirror-polished bulk Ti, sputter-deposited Ti, and PS dish. The data were normalized to the GAPDH housekeeping gene. The data are the mean ± SD; $n = 3$; $^{*}p < 0.05$.

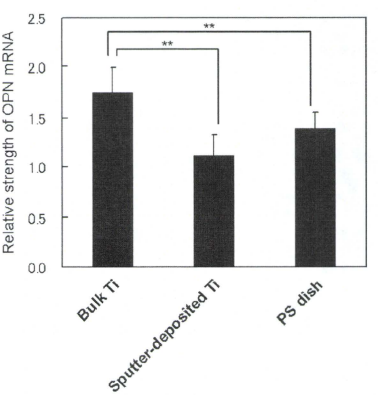

FIGURE 8. OPN gene expression analysis of MC3T3-E1 cells differentiation-induced for 10 days on mirror-polished bulk Ti, sputter-deposited Ti, and PS dish. The data were normalized to the GAPDH housekeeping gene. The data are the mean ± SD; $n = 3$; $^{**}p < 0.01$.

plastic dish.[22] In this study, no significant differences in the numbers of attached cells among three experimental lines were observed, while the bone differentiation properties were greater on the bulk Ti than on the sputter-deposited Ti. Therefore, the bone differentiation properties in osteogenic cells may not correlate with the cell proliferation. On the other hand, the tiny differences in the surface conditions between the bulk Ti and the sputter-deposited Ti influence the osteogenic differentiation properties. It is important to understand the surface conditions of materials that are used for cell culture tests.

CONCLUSIONS

There were no significant differences in the cell morphology and attached number of MC3T3-E1 cells cultured on the bulk and sputter-deposited Ti for 3 days. After differentiation induction, the time showing maximum activity in the ALP on the bulk Ti was superior to those on the sputter-deposited Ti. Furthermore, the cells on the bulk Ti were also better than those on the sputter-deposited Ti in the gene expression analysis. There was no significant difference in the surface roughness between the bulk and sputter-deposited Ti. However, the surface of the sputter-deposited Ti was more uniform and cleaner than that of the bulk Ti. On the other hand, the thickness of surface oxide film on the sputter-deposited Ti was smaller than that on the bulk Ti. Moreover, the composition of the oxide film was also different: The proportions of TiO and Ti_2O_3 in the surface oxide film on the sputter-deposited Ti were larger than those on the bulk Ti. These differences might influence the differentiation of MC3T3-E1 cells.

REFERENCES

1. Thull R, Grant D. Physical and chemical vapor deposition and plasma-assisted techniques for coating titanium. In: Brunette DM, Tengvall P, Textor M, Thomsen P, editors. Titanium in Medicine. Heidelberg: Springer; 2001. p 283–341.
2. Asami K. A precisely consistent energy calibration method for X-ray photoelectron spectroscopy. J Electron Spectrosc 1976;9: 469–478.
3. Livak KJ, Schmittgen TD. Analysis of relative gene expression data using real-time quantitative PCR and the $2^{-\Delta\Delta C_t}$ method. Methods 2001;25:402–408.
4. Asami K, Chen SC, Habazaki H, Hashimoto K. The surface characterization of titanium and titanium-nickel alloys in sulfuric acid. Corros Sci 1993;35:43–49.
5. Asami K, Hashimoto K. The X-ray photo-electron spectra of several oxides of iron and chromium. Corros Sci 1977;17:559–570.
6. Kuboki Y, Kudo A, Mizuno M, Kawamura M. Time-dependent changes of collagen cross-links and their precursors in the culture of osteogenic cells. Calcif Tissue Int 1992;50:473–480.
7. Beck GR, Sullivan EC, Moran E, Zerler B. Relationship between alkaline phosphatase levels, osteopontin expression, and mineralization in differentiating MC3T3-E1 osteoblasts. J Cell Biochem 1998;68:269–280.
8. Stein GS, Lian JB, Owen TA. Relationship of cell growth to the regulation of tissue-specific gene expression during osteoblast differentiation. FASEB J 1990;4:3111–3123.
9. Stein GS, Lian JB, van Wijnen AJ, Stein JL, Montecino M, Javed A, Zaidi SK, Young DW, Choi JY, Pockwinse SM. Runx2 control of organization, assembly and activity of the regulatory machinery for skeletal gene expression. Oncogene 2004;24:4315–4329.
10. Aghaloo T, Cowan CM, Chou YF, Zhang X, Lee H, Miao S, Hong N, Kuroda S, Wu B, Ting K, Soo C. Nell-1-induced bone regeneration in calvarial defects. Am J Pathol 2006;169:903–915.
11. Setzer B, Bächle M, Metzger MC, Kohal RJ. The gene-expression and phenotypic response of hFOB 1.19 osteoblasts to surface-modified titanium and zirconia. Biomaterials 2009;30:979–990.
12. Mckee MD, Farach-Carson MC, Butler WT, Hauschka PV, Nanci A. Ultrastructural immunolocalization of noncollagenous (osteopontin and osteocalcin) and plasma (albumin and alpha 2HS-glycoprotein) proteins in rat bone. J Bone Miner Res 1993;8:485–496.
13. Mckee MD, Nanci A. Osteopontin: An interfacial extracellular matrix protein in mineralized tissues. Connect Tissue Res 1996;35: 197–205.
14. Mckee MD, Nanci A. Osteopontin at mineralized tissue interfaces in bone, teeth, and osseointegrated implants: Ultrastructural distribution and implications for mineralized tissue formation, turnover, and repair. Microsc Res Tech 1996;33:141–164.
15. Hiromoto S, Hanawa T, Asami K. Composition of surface oxide film of titanium with culturing murine fibroblasts L929. Biomaterials 2004;25:979–986.
16. Sundgren JE, Bodö P, Ivarsson B, Lundström I. Adsorption of fibrinogen on titanium and gold surfaces studied by ESCA and ellipsometry. J Colloid Interface Sci 1986;113:530–543.
17. Lide DR. CRC Handbook of Chemistry and Physics, 87th ed. Boca Raton: CRC press; 2006. p 6–136.
18. Martin JY, Schwartz Z, Hummert TW, Schraub DM, Simpson J, Lankford J. Effect of titanium surface roughness on proliferation, differentiation, and protein synthesis of human osteoblast-like cells (MG63). J Biomed Mater Res 1995;29:389–401.
19. Kieswetter K, Schwartz Z, Hummert TW, Cochran DL, Simpson J, Dean DD, Boyan BD. Surface roughness modulates the local production of growth factors and cytokines by osteoblast-like MG-63 cells. J Biomed Mater Res 1996;32:55–63.
20. Boyan BD, Batzer R, Kieswetter K, Liu Y, Cochran DL, Szmuckler-Moncler S, Dean DD, Schwartz Z. Titanium surface roughness alters responsiveness of MG63 osteoblast-like cells to 1 alpha,25-$(OH)_2D_3$. J Biomed Mater Res 1998;39:77–85.
21. Webster TJ, Ejiofor JU. Increased osteoblast adhesion on nanophase metals: Ti, Ti6Al4V, and CoCrMo. Biomaterials 2004;25: 4731–4739.
22. Schneider GB, Perinpanayagam H, Clegg M, Zaharias R, Seabold D, Keller J, Stanford C. Implant surface roughness affects osteoblast gene expression. J Dent Res 2003;82:372–376.

Effects of electrodeposited poly(ethylene glycol) on biofilm adherence to titanium

Yuta Tanaka,[1] Khairul Matin,[2] Mariko Gyo,[2] Ayako Okada,[2,3] Yusuke Tsutsumi,[1] Hisashi Doi,[1] Naoyuki Nomura,[1] Junji Tagami,[2,4] Takao Hanawa[1,5]

[1]Department of Metals, Institute of Biomaterials and Bioengineering, Tokyo Medical and Dental University, Chiyoda-Ku, Tokyo, Japan
[2]Cariology and Operative Dentistry, Department of Restorative Sciences, Graduate School, Tokyo Medical and Dental University, Tokyo, Japan
[3]Department of Translational Research, School of Dental Medicine, Tsurumi University, Tsurumi, Yokohama, Japan
[4]Global Center of Excellence (G-COE) Program, International Research Center for Molecular Science in Tooth and Bone Diseases at Tokyo Medical and Dental University, Tokyo, Japan
[5]Graduate School of Engineering, The University of Tokyo, Bunkyo-Ku, Tokyo, Japan

Received 1 January 2010; revised 19 March 2010; accepted 21 May 2010
Published online 28 September 2010 in Wiley Online Library (wileyonlinelibrary.com). DOI: 10.1002/jbm.a.32932

Abstract: Protein-resistant coatings have been studied for inhibiting biofilm formation on implant devices. In this study, titanium (Ti) surfaces were biofunctionalized with poly(ethylene glycol) (PEG) by electrodeposition and were evaluated as biofilm substrates under an oral simulated environment. *Streptococcus gordonii*, an early colonizer of oral biofilms, was inoculated on Ti and PEG-electrodeposited Ti (PEG-Ti) surfaces and was analyzed quantitatively and topographically. *Streptococcus mutans* supplemented with sucrose, a late colonizer mainly found in dental plaque, was also used to form biofilms on the surfaces of Ti and PEG-Ti for 20 h followed by sonication as a means of detaching the biofilms. The results indicated that the attachment of *S. gordonii* on PEG-Ti surfaces was inhibited compared with Ti, and the *S. mutans* biofilm was easier to be detached from the surface of PEG-Ti than that of Ti. Moreover, the presence of PEG electrodeposited on Ti surface inhibited salivary protein adsorption. The degree of detachment of biofilms from PEG-Ti was associated with the inhibition of the salivary protein adsorption, suggesting weak basal attachment of the biofilms to the electrodeposited surfaces. Therefore, controlling protein adsorption at the initial stage of biofilm formation may be an effective strategy to protect metal surfaces from bacterial contamination not only in dental manipulations but also in orthopedic applications. © 2010 Wiley Periodicals, Inc. J Biomed Mater Res Part A: 95A: 1105–1113, 2010.

Key Words: titanium, poly(ethylene glycol), surface treatment, protein adsorption, bacterial adhesion, biofilm

INTRODUCTION

Some odontopathologies are caused by interactions between the implant or restorative materials and bacteria in the oral cavity. In the case of dental implants, the bacteria may enter into postoperative implanted sites, causing infections such as peri-implantal diseases.[1–3] These infections are important issue not only in dental manipulations but also in orthopedic applications such as spinal fixations devices.[4] The risk of infections caused by resistant pathogens such as methicillin-resistant *Staphylococcus aureus* is particularly high in patients with hip prosthesis, implanted spinal, or vascular devices.[5,6]

In recent years, biofilm formation as well as simple bacterial adhesion onto implanted metal surfaces has been considered major routes of infection in the oral cavity. Biofilm formation is a multifactorial complicated process, occasionally referred to as a two-step process requiring initial bacterial adhesion to the surface followed by the bacteria–bacteria intercommunication leading to the formation of multiple layers of bacteria.[7] In addition, glucans and fructans are the major extracellular polysaccharides produced by oral streptococci, serving as reserves of energy and enabling the cells to adhere to the tooth surface. *Streptococcus mutans* colonize the tooth surface via both sucrose-dependent and independent mechanisms.[8] In the presence of sucrose, the glucosyltransferase enzymes produce water-insoluble glucan (WIG) polymers encoded by the products of the *gtfB* and *gtfC* genes, which play key roles in adhesion and accumulation (formation) of biofilms.[9] Once biofilms have formed, it becomes very difficult to eliminate the glucan-embedded pathogens because the bacteria in the interior of the biofilm remain protected from disinfectants and even from strong antibiotics. Therefore, a bacterial attachment-resistant surface or a surface that would allow the removal of biofilms with disinfectants or by applied physical forces (sonication, etc.) is required for maximally efficient biomaterials.

The most common strategy to prevent the formation of biofilms on metallic devices is to polish the metal surface because roughening of material surface is known to enhance bacterial adhesion because of the increase in the surface

Correspondence to: K. Matin; e-mail: matin.ope@tmd.ac.jp or T. Hanawa; e-mail: hanawa.met@tmd.ac.jp

area and the formation of pockets for harboring bacteria.[10,11] Coating titanium (Ti) with nitrogen or silver (Ag) ions has also been investigated. Ti nitride coatings minimize the adhesion of *S. mutans* and *Pseudomonas aeruginosa*.[12] Ag nitrated coatings have also been studied for years because Ag ion is known to exhibit antibacterial properties.[13] Stainless steel pins coated with Ag have been found to decrease the adhesion and colonization of *S. aureus*, *Staphylococcus epidermidis*, and *P. aeruginosa* around the coated implant.[14,15] However, there are also reports that Ag is toxic to host cells, causing severe toxic reactions.[16,17] Protein-resistant coatings are considered to be most useful for the inhibition of the biofilm formation because protein adsorption usually initiates this process on implant surfaces.

Recently, the immobilization of functional molecules or biomolecules on the metal surfaces has become popular to create protein-resistant surfaces. Immobilization of poly(ethylene glycol) (PEG) on material surfaces is the preferred strategy for inhibiting protein adsorption. Among methods reported on the immobilization of PEG on metal surfaces, graft copolymers of poly(L-lysine) and PEG (PLL-*g*-PEG) have proven to be particularly effective for rendering metal surfaces highly resistant to nonspecific protein adsorption.[18] However, this method includes multistage processes for the synthesis of PLL-*g*-PEG and immobilization by immersion. Therefore, a simple and universal immobilization technique for all metals is necessary. In this study, we attempted to immobilize PEG terminated with amines at both ends of the polymer (NH_2-PEG-NH_2) onto metals by electrodeposition, which is considered to be simple and universal for electroconductive materials and those with a complex morphology. Previous studies reported electrodeposited surface inhibited albumin adsorption and platelet adhesion,[19,20] but the behavior of electrodeposited PEG against bacterial adherence and biofilm formation has not been examined.

The oral biofilm formation on materials (specifically dental materials and oral biomaterials) has been currently studied *in vitro* by simulating the human oral environment.[10,21,22] Evaluation of the PEG-electrodeposited Ti surface under an oral simulated environment would certainly be helpful in terms of obtaining data simply with minimization of possibly confounding variable factors. Moreover, the role of dental bacterium on the biofilm formation followed by infections is becoming increasingly clear relative to those of *S. aureus* or *S. epidermidis* around orthopedic implant. Therefore, the purpose of this study was to investigate dental bacterial adhesion directly as well as biofilm formation on PEG-electrodeposited Ti surfaces relative to untreated Ti *in vitro*.

MATERIALS AND METHODS

Specimen preparation and immobilization of PEG by electrodeposition

A commercially pure titanium disk (Ti; 5 mm in diameter and 2 mm in thickness) of grade 2 (Rare Metallic Co., Inc., Japan) was mirror-polished (Ti_S) with silicon carbide paper (SiC), 9-μm diamond suspension, and 0.04-μm colloidal silica suspension for surface characterization, biofilm formation, or salivary protein adsorption. Ti (Ti_R) polished with 800-SiC paper after mirror-polishing for bacterial adhesion or biofilm formation was also prepared. A 99.99% Ag disk (5 mm in diameter and 2 mm in thickness; Rare Metallic Co., Inc., Japan) was mirror-polished (Ag_S) with SiC paper, 3-μm diamond suspension, and 0.05-μm colloidal alumina suspension for use as a negative control because Ag ion is known to exhibit antibacterial properties. Furthermore, Ag polished with 800-SiC paper (Ag_R) was also prepared. These disks were cleared of macroscopic contamination by sonication in acetone for 15 min, dried with a stream of nitrogen (99.9%), and stored in a desiccator until immobilization with PEG.

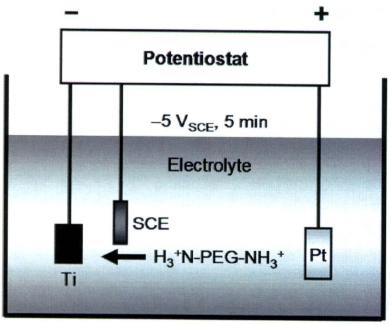

FIGURE 1. Schematic illustration of PEG electrodeposition on pure Ti surface. During cathodic polarization, NH_2-PEG-NH_2 migrated to the cathode Ti surface, where they were immobilized. The 2mass% NH_2-PEG-NH_2 solution with 0.3 mol L^{-1} NaCl solution was used as the electrolyte.

The PEG molecules used in this study were characterized by termination with NH_2 (NH_2-PEG-NH_2; MW = 1000, PEG1000 Diamine, NOF Corp., Japan) at both terminals of the molecule. NH_2-PEG-NH_2 was dissolved in 0.3 mol L^{-1} NaCl solution at a concentration of 2mass%. The resulting solution was used as an electrolyte for electrodeposition at 310 K. The open circuit potential of Ti relative to a saturated calomel electrode (SCE) before electrodeposition was measured. Thereafter, a cathodic potential was applied from the open circuit potential with a constant sweep rate of −0.1 V s^{-1} and maintained at −5.0 V_{SCE} for 5 min. During cathodic polarization, NH_2-PEG-NH_2 migrated to the cathodic Ti, where they were immobilized as shown in Figure 1. After electrodeposition, each specimen was rinsed in deionized water and dried under flowing nitrogen (99.9%).

Characterization of PEG layer immobilized on Ti by X-ray photoelectron spectroscopy

The chemical bonding states existing in the PEG layer immobilized by electrodeposition were characterized using X-ray photoelectron spectroscopy (XPS) (SSX100, Surface Science Instrument). For comparison, Ti_S electrodeposited (−5.0 V_{SCE}, 5 min) in 0.3 mol L^{-1} NaCl solution without NH_2-PEG-NH_2 at 310 K was characterized. All binding

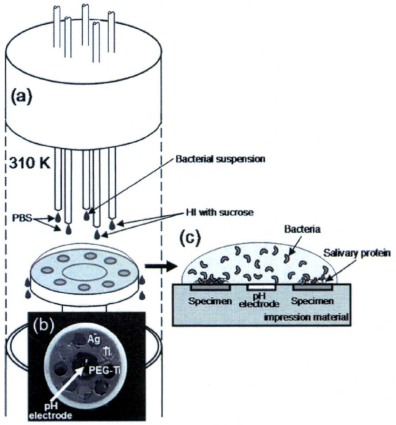

FIGURE 2. (a) Schematic diagram of a chamber of the OBR. (b) Specimens fixed using a hydrophilic vinyl polysiloxane impression material. (c) Biofilm formation on specimen surfaces that occurred in an underwater environment. HI, heart infusion broth.

energies given in this article are relative to the Fermi level, and all spectra were excited with the monochromatized Al Kα line (1486.61 eV). The spectrometer was calibrated against Au $4f_{7/2}$ (84.07 eV) and Au $4f_{5/2}$ (87.74 eV) of pure gold and Cu $2p_{3/2}$ (932.53 eV), Cu $2p_{1/2}$ (952.35 eV), and a Cu Auger $L_3M_{4,5}M_{4,5}$ line (918.65 eV) of pure Cu. The energy values were based on published data.[23] The take-off angle for photoelectron detection was 35° from the surface of the specimen. To estimate the photoelectron peak intensities, the background was subtracted from the measured spectrum according to Shirley's method.[24]

Preparation of bacterial suspensions

Suspensions of *S. gordonii* ATCC10558 in phosphate-buffered saline (PBS) at OD_{500} = 0.1 and *S. mutans* MT8148 at OD_{500} = 2.0 were prepared from 16-h fresh cultures in brain heart infusion broth (Becton Dickinson, Sparks, MD) after washing two times with PBS. To assess initial bacterial attachment, *S. gordonii* planktonic cell suspensions were used. For biofilm formation-resistant studies, *S. mutans* was used with a solution of heart infusion broth (Becton Dickinson) with sucrose (0.1% final concentration).

Specimen assembly and biofilm formation in the oral biofilm reactor

As described previously, metal specimens were assembled on the polytetrafluoroethylene holder of each oral biofilm reactor (OBR) chamber [Fig. 2(a)] around a flat pH electrode[10,21,22] and fixed horizontally using a hydrophilic vinyl polysiloxane impression material (Exafine regular type, GC, Tokyo, Japan), as shown in Figure 2(b). As a result, the upper surface of each specimen remained exposed (exposed area = 19.6 mm^2) for biofilm attachment. The two experiments, (1) planktonic bacterial attachment without sucrose using *S. gordonii* and (2) sucrose-dependent biofilm formation using *S. mutans*, were performed on two separate sets of specimens. For *S. mutans* biofilm study, pooled sterile human saliva was then poured onto the specimens followed by incubation for 30 min to obtain a coat of salivary pellicle on the specimens. All volunteers who generously provided saliva were given informed consent on the experimental protocol, which was approved by the Research Ethics Committee of Tokyo Medical and Dental University Faculty of Dentistry.

The procedures in common were as follows: the holders were placed on a silicon plug at the bottom of the chamber. The top of the chamber was sealed with a silicon plug so that the chamber itself in Figure 2(a) served as an incubator with a 310 K internal temperature. The top silicon plug was equipped with five stainless steel tubes (21 gauge), which were separately connected to five silicon tubes to collect bacterial suspensions and other solutions via computer-controlled roller pumps (EYELA EPC-2000; Tokyo Rika, Tokyo, Japan). *S. gordonii* suspension was dropped for 2 h onto the center of the holder via one of the silicon tube to directly observe planktonic bacterial attachment. For biofilm formation, one tube for the *S. mutans* suspension, two for heart infusion broth with sucrose, and the other two for PBS were used. All of these solutions were pumped into the chambers at 6 mL h^{-1} for 20 h. The solutions formed a water dome on the surface of the holder, which was continuously stirred by the falling drops, as shown in Figure 2(c). When the water dome reached its maximum height, the mixture of excess liquid overflowed from the edge of the holder. Two chambers were used at the same time to confirm experimental stability. During the experiment, the pH on the surface of the holder was continuously monitored and recorded.

In situ quantification of attached bacterial cells

Attached *S. gordonii* cells on specimen surfaces were quantified after staining with LIVE/DEAD® *Bac*Light™ Bacterial Viability Kits (Molecular Probes; Invitrogen, Carlsbad, CA). Immediately after removal from the OBR, the specimens were rinsed with PBS, stained with *Bac*Light, and inspected using a fluorescence microscope (CKX41; Olympus, Tokyo, Japan). The number of *S. gordonii* cells remaining attached on the specimens was counted with fluorescence microscopic images.

Quantitative assessment of the biofilms formed on the specimens

S. mutans biofilm formation on the mirror-specimens in the OBR was quantitatively assessed. The specimens with 20-h artificial biofilms were removed from the holder in the OBR and were rinsed with PBS. After that, loosely attached biofilms on specimens were removed by sonication (UP50H, hielscher; Dr. Hielscher GmbH, Stuttgart, Germany) forces at

10, 20, and 30 W. The specimens were then incubated in 1 mL of 0.5 mol sodium hydroxide solutions (NaOH) individually using microtubes for 15 min and vortex agitated for 15 s to detach the adherent biofilms from the specimens and dissolve the WIG matrix. The quantity of dissolved WIG was measured with the phenol-H_2SO_4 method.[25] The WIG solution (500 μL) from each specimen was disintegrated with phenol-H_2SO_4, and 200 μL of each WIG was subjected to estimation of the quantity of WIG (μg mL^{-1}) using a Biotrak II Plate reader (OD_{492}). To obtain a standard glucose curve, 0, 25, 50, 75, 100, 150, and 200 μg mL^{-1} of glucose were also assayed at OD_{492}.

Morphological study of the biofilms by scanning electron microscope

Initial attachment of *S. gordonii* and *S. mutans* biofilm formation on each surface were observed with a scanning electron microscope (SEM; S-3400NX, Hitachi, Japan). The specimens were removed from the chamber, rinsed with PBS, and fixed in 4% paraformaldehyde with 1% glutaraldehyde in PBS for 1 h. They were then rinsed with PBS, dehydrated through a series of ethanol (50, 60, 70, 80, 90, and 100vol%) washes, desiccated, and sputter-coated using gold (SC-701AT; Elionix, Tokyo, Japan). Each of the specimens was inspected, and photomicrographs were taken using the SEM.

Salivary protein quantification and electrophoresis of protein

The Ag_S, Ti_S, and PEG-Ti_S were immersed in saliva for 2 h to quantify initial adsorbed proteins. After 2 h, the physically adsorbed saliva on each specimen was removed with Milli-Q water (Millipore) with shaking (5 min, 50 min^{-1}, three times). The retained salivary proteins were fully desorbed by vortexing in extraction buffer [urea 10% (w/v), sodium dodecyl sulfate (SDS) 20% (v/v), Triton X-100, dithiothreitol, pharmalyte 3-10; Millipore] and quantified at 280 nm with a spectrophotometer (Protein A280; NanoDrop Technologies, Inc., Wilmington, DE). SDS-polyacrylamide gel electrophoresis (SDS-PAGE) was performed with a precast 3–10% gel gradient (PAGEL NPG-310L; Atto Corp., Tokyo, Japan). The PAGE allows protein separation by differential migration to the anode or cathode through a nonreactive matrix formed by acrylamide and *N,N*-methylene bisacrylamide cononomers that undergo free radical-mediated polymerization. The retained salivary proteins were separated on the gradient gels in electrophoresis buffer (0.1% SDS, 192 mmol L^{-1} glycine, and 25 mmol L^{-1} Tris) at a constant current (20 mA) for 90 min. A Mark12™ Unstained Standard molecular weight marker was included in each run. The gels were stained with Ag stain kit (AE-1360 EzStain Silver, Atto Corp.), scanned with a luminescent image analyzer (LAS-3000; Fujifilm, Tokyo, Japan), and saved as TIFF files.

Statistical analysis

Statistical comparisons were preformed using the one-way factorial analysis of variance, including the interaction effect and *post-hoc* Tukey's multiple comparison testing.

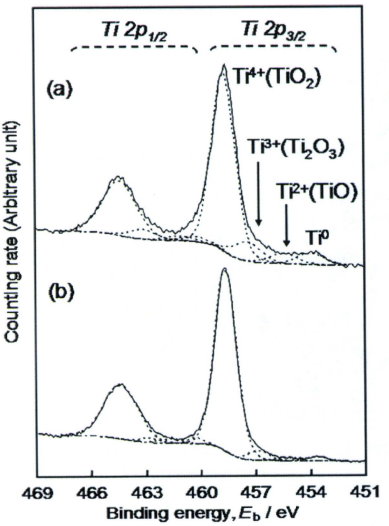

FIGURE 3. The Ti 2p spectra obtained from Ti surfaces electrodeposited into the electrolytes. (a) NaCl solution without NH_2-PEG-NH_2. (b) NaCl solution with NH_2-PEG-NH_2.

RESULTS

Characterization of PEG layer electrodeposited on Ti

The Ti 2p spectra obtained from Ti surfaces electrodeposited into the electrolytes (NaCl solutions) with NH_2-PEG-NH_2 and without NH_2-PEG-NH_2 are shown in Figure 3 and gave four peaks according to valence; Ti^0 (metallic state), Ti^{2+} (TiO), Ti^{3+} (Ti_2O_3), and Ti^{4+} (TiO_2). The metallic and oxide states were detected from both specimens, and the fraction of Ti^0 in electrodeposited Ti into the solution with NH_2-PEG-NH_2 was smaller than that without NH_2-PEG-NH_2.

Bacteria adhered to the specimens

The WIG-free *S. gordonii* colonies were formed on Ag_R, Ti_R, and PEG-Ti_R for 2 h in the OBR. *Bac*Light staining images obtained from each specimen are shown in Figure 4(a). Live *S. gordonii* cells were visualized as green and dead cells as red in the same microscopic location on each surface after a change of emission filters. Most of cells on PEG-Ti_R were barely alive, perhaps cells were about to die as they were visualized yellowish instead of green. The total number of live and dead cells counted from fluorescence photomicrography was significantly less on PEG-Ti_R than on Ti_R, as shown in Figure 4(b). The results of SEM images in Figure 4(c) corresponded with those of fluorescence photomicrography. Also, the number of *S. gordonii* was less on Ag_R (negative control) than on Ti_R or PEG-Ti_R as shown in Figure 4.

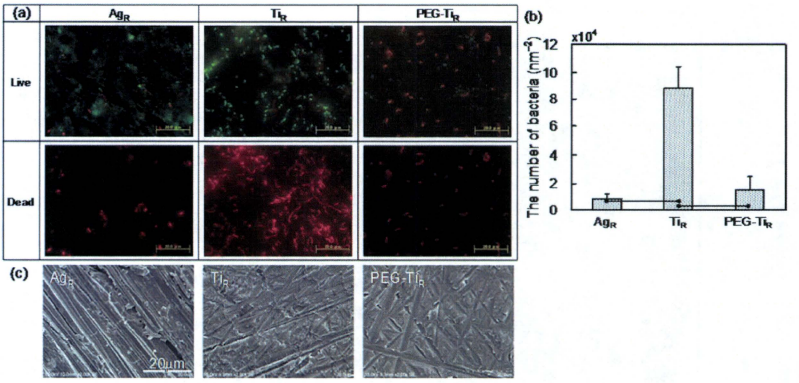

FIGURE 4. The amount of *S. gordonii* cells adhered on the rough surfaces of Ag (Ag_R), untreated Ti (Ti_R), and electrodeposited Ti (PEG-Ti_R). (a) Fluorescence photomicrograph of *S. gordonii* cells stained with *Bac*Light Bacterial Viability Kit. (b) The number of cells counted from fluorescence photomicrographs. The bars represent statistically significant differences ($p < 0.01$). (c) SEM images of *S. gordonii* cells on the surfaces of the metals. All data indicate and reconfirm that Ag had minimum *S. gordonii* cells got attached on its surface, uncoated Ti had maximum, and PEG-Ti had in between, but significantly less compared with Ti.

Quantity of glucan in the biofilm formed on specimen surfaces

Sucrose-dependent biofilms are generally formed on the surfaces dependent on superadherent WIG. The quantity of WIG in the retained *S. mutans* biofilm after sonication was evaluated as an indicator of biofilm adherence. The concentration of WIG in biofilms retained after 10, 20, and 30-W sonication was almost identical for Ti_S and PEG-Ti_S, as shown in Figure 5. Most of the biofilms on both specimens were detached by 10-W sonication. Contrary to all expectations, the concentration of WIG was significantly more abundant on Ag_S than on Ti_S and PEG-Ti_S. The concentration of WIG decreased with the increase in the sonication levels. In the case of surfaces polished with 800-SiC paper, the concentration of WIG in the retained biofilms after 30-W sonication was less on PEG-Ti_R than on Ti_R, as shown in Figure 6.

Amount of adsorbed saliva and salivary protein separation

The amount of salivary proteins adsorbed on Ag_S was significantly higher than those of Ti_S and PEG-Ti_S, as shown in Figure 7(a). In contrast, lesser amounts of salivary proteins were adsorbed on PEG-Ti_S than on Ti_S, although the difference did not reach the significance level. SDS-PAGE analysis showed a single band of about 52 kDa from each specimen, reproducibly, as shown in Figure 7(b). This band seemed to be amylase because its molecular mass is near 52 kDa. These bands on SDS-PAGE were visualized in the following order: Ag_S, Ti_S, and PEG-Ti_S. The band of the 52-kDa salivary protein was barely visible in the PEG-Ti_S lane, which was stronger in the Ti_S lane and strongest in the Ag_S lane.

DISCUSSION

The photoelectron signals detected by XPS from a deep site are weak because they decay while passing through molecules and solids. In other words, the smaller the fraction of Ti^0 (metallic state just under TiO_2) is, the thicker the deposited layer on TiO_2 is. This means few deposited layer was formed on TiO_2 in electrodeposited into the NaCl solution without NH_2-PEG-NH_2, whereas thin layer was formed on TiO_2 in the solution with NH_2-PEG-NH_2. The thin layer was characterized using ellipsometry, XPS with an angle-resolved technique, glow discharge optical emission spectroscopy, and

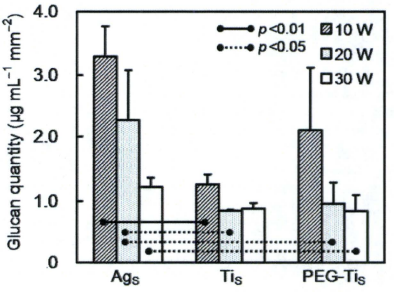

FIGURE 5. The amount of WIG in biofilms retained on the smooth surfaces of Ag (Ag_S), untreated Ti (Ti_S), and electrodeposited Ti (PEG-Ti_S) after 10, 20, and 30-W sonication. The bars represent statistically significant differences.

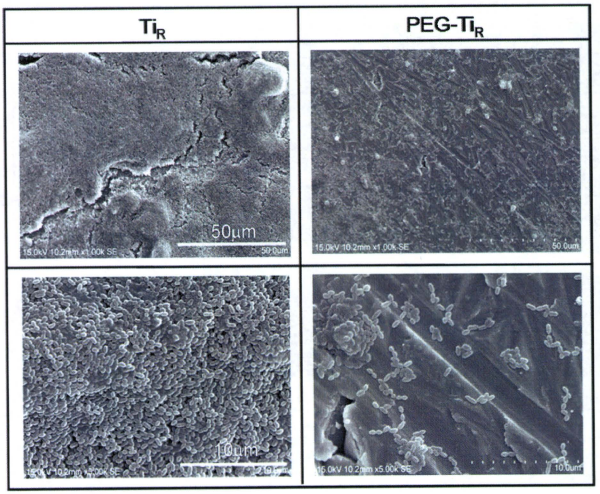

FIGURE 6. SEM images of the retained *S. mutans* biofilms on the rough surfaces of untreated Ti (Ti_R) and electrodeposited Ti ($PEG\text{-}Ti_R$) after 30-W sonication. A thick layer of *S. mutans* biofilm was retained on untreated Ti. Compared with the latter, only few scattered colonies were retained on PEG-electrodeposited Ti, and most of the biofilms were detached on sonication.

Fourier transform infrared reflection absorption spectroscopy in detail in previous studies.[19,20,26,27] As a result, electrodeposition technique led to the immobilization of NH_2-PEG-NH_2 onto the Ti surface. More terminated amines combined with hydroxyl groups on TiO_2 as a stable bonding and formed U-shaped conformation of PEGs looped onto the Ti surface relative to conventional immersion technique (unstable interfacial bonding and random conformation). The durability of electrodeposited PEGs seem to be high because they were not desorbed into platelet solution, cellular medium, and shake water and expressed biofunctions.[20,28,29]

In this study, attachment of WIG-free *S. gordonii* and biofilms of *S. mutans* onto untreated and PEG-Ti surfaces were observed to clarify the behaviors of initial attachment and biofilm formation, respectively. *S. gordonii* preferentially attached on proteins initially adsorbed on the implanted material,[30] whereas *S. mutans* is a late colonizer mainly found in dental plaque and is associated with dental caries, which is unusable for the evaluation of initial attachment of bacteria. WIG is considered to be critically important in biofilm formation because it is insoluble in water and also possesses a marked ability to promote adherence when synthesized *de novo* on various solid surfaces.[8] Because the ability to produce WIG is known to be almost free for *S. gordonii*, biofilms formation by *S. gordonii* will have weaker adherence on the specimens than those by *S. mutans*. Hence, biofilm adherence was evaluated by the quantification of WIG synthesized by *S. mutans*.

PEG-Ti surfaces inhibited the attachment of *S. gordonii* and, consequently, colony formation in this study. The static stabilization and excluded-volume effects[31,32] of PEG immobilized on the materials results in the inhibition of protein adsorption in general. In addition, as the both terminals of PEGs remain immobilized on the Ti surface, no charges would be expected on the U-shaped PEG loops. Hence, bacterial attachment (attachment of cell surface proteins of bacteria) and subsequent colony formation of bacteria was inhibited or weakened on the PEG-Ti surface because of the steric stabilization or excluded-volume effects of PEGs.

The properties of *S. gordonii* would have allowed preferential attachment of the organisms to proteins adsorbed initially on the implanted materials (acquired pellicle). The cell surface proteins function as coaggregation receptors for cell–cell communication in the oral biofilm community. Rogers et al.[33] reported that the AbpA (amylase-binding proteinA or SspA, SspB) of *S. gordonii* cells seems to play a role in the adhesion of this bacterium to amylase in the acquired enamel pellicle. If this protein adsorption at the initial stage can be inhibited, colony formation after *S. gordonii* attachment and eventual biofilm formation could be inhibited. Therefore, adsorption of salivary proteins onto the PEG-Ti surface was also investigated in this study. The mirror-polished surfaces were used for quantification of adsorbed proteins. Our results showed that the $PEG\text{-}Ti_S$ surface inhibited saliva adsorption relative to untreated Ti_S. Further,

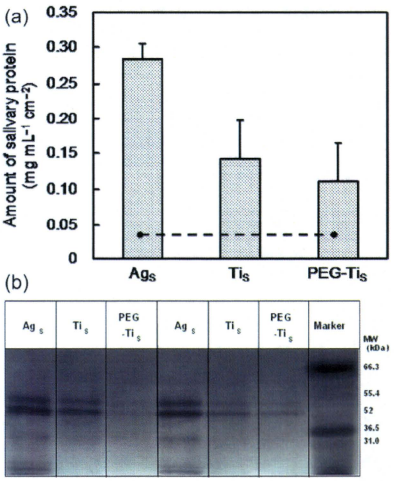

FIGURE 7. (a) The amounts of adsorbed salivary proteins on the smooth surfaces of Ag (Ag_S), untreated Ti (Ti_S), and electrodeposited Ti (PEG-Ti_S) measured using a spectrophotometer. (b) SDS-PAGE analysis of salivary proteins on the smooth surfaces of Ag (Ag_S), untreated Ti (Ti_S), and electrodeposited Ti (PEG-Ti_S). The dashed bars represent statistically significant differences ($p < 0.05$). These bands on SDS-PAGE were emphasized in the following order: Ag_S, Ti_S, and PEG-Ti_S. The band of 52-kDa salivary protein appeared almost fading in PEG-Ti_S lane, which is thicker in Ti lane and thickest in Ag_S lane.

SDS-PAGE analysis indicated that a salivary protein with a molecular size of 52-kDa weakly bound to PEG-Ti_S and was more strongly bound to Ti_S lane and even more tightly to Ag_S. This protein is considered to be amylase because its molecular mass is near 52 kDa. Approximately 60% of human salivary proteins are known to be amylase, which is randomly available in the acquired pellicle and plays a major role in the early attachment of several oral streptococci, including *S. gordonii*. Evidently, the adsorption of amylase was inhibited by PEG loops electrodeposited on Ti in this study, and this might account for the weaker *S. mutans* biofilm formation. One of the reasons behind this weak aggregation might be failure in acquiring the additional attractive electrostatic force that promote adhesion of *S. mutans* cell surface antigen I/II to saliva-coated surfaces via salivary proteins[34] because the movements (fluctuations) of the looped PEG molecules may interfere to generate the electrostatic interaction.

Sucrose-dependent *S. mutans* biofilm formation indicates stronger colony formation by the bacteria and enhancement of biofilm adherence by extracellular polysaccharides or WIG deposition. With a supplement of sucrose, the *S. mutans* cells used in this study become more strongly adherent in the presence of WIG during biofilm formation. It might be noteworthy that to obtain homogenous biofilms with reproducibility in adherence by similarly produced WIG in all experiments, this study was restricted to single-species biofilms rather than using consortium biofilms. The laboratory strain *S. mutans* MT8148 is known to be capable of producing three major glucosyltransferases and an optimum proportion of each is necessary for maximum sucrose-dependent adherence of the bacteria.[9]

No differences could be detected when the quantity of *S. mutans* cells and glucan were measured from the surfaces of untreated and treated Ti specimens. This might be because the bacteria (*S. mutans*) attempt to attach as soon as they are spread inside the dome-shaped liquid over the Ti specimens in the OBR and instantly begin to proliferate and metabolize sucrose. Through a series of metabolic activities, they ferment sucrose and produce glucans around the cell bodies to form more adherent biofilms. Also, Delmi et al.[35] and Ha et al.[36] reported extensive *S. aureus* and *S. epidermidis* cell adhesion and biofilm formation on Ti alloys compared with stainless steel, whereas Gracia et al.[37] found no significant differences between adhesion of *S. aureus* to Ti alloy and stainless steel surfaces. The degree of biofilm formation might be different dependent on the experimental environment and surface conditions such as surface roughness, surface charge, and surface composition. Therefore, the biofilms retained after sonication were evaluated in this study.

The concentration of WIG retained in the biofilms was measured as shown in Figure 5. No significant differences could be detected between the untreated and electrodeposited Ti_S at any of the applied sonication forces. Almost all of the biofilms were detached by sonications at 20 and 30 W. These results indicated that the biofilms were more readily detached from Ti_S compared with that of Ag_S.

Tanner et al.[38] reported that the rougher material promoted biofilm accumulation significantly more than smoother materials. Moreover, the difference in protein adsorption between Ti_S and PEG-Ti_S is expected owing to the increase of surface areas. In this study, retained biofilms on PEG-Ti were also observed. The degree of biofilm formation was increased by roughening the surface. Consequently, the degree of retained biofilm was less on the PEG-Ti than on the untreated one despite no difference in the mirror surfaces, as shown in Figure 6. In other words, even if the surface was roughened, the immobilization of PEG on Ti was effective in allowing for the detachment of the biofilm.

In this study, the specimens were coated with saliva to form an acquired pellicle. The adhesion of bacteria and biofilm formation is considered to be associated with the proteins in the saliva. *Prophyromonas gingivalis* and other periodontal pathogens accumulate in periodontal and peri-implantal biofilms as late colonizers after *S. gordonii* form the initial layers on proline-rich glycoproteins and other similar proteins of the acquired pellicle.[39] Therefore, the attenuation of the formation of peri-implantal biofilms on PEG-Ti is possible as a consequence of the inhibition of the saliva adsorption. Actually, the biofilm was easier to detach from the PEG-Ti surface because the PEG immobilization may have inhibited the protein (e.g., α-amylase) adsorption

more than on the untreated one. At pH levels lower than pH 6, the extracellular polysaccharides and bacteria are negatively charged, whereas salivary amylase (pH = 5.6–6.4) is positively charged based on titration curves.[40] Therefore, bacteria and WIG are strongly attracted to the adsorbed proteins because of these electrostatic attractions. If the biofilm was detached with an external force, the detached interface might include the Ti surface and proteins. This means that the degree of detachment of biofilms is associated with the proteins adsorption and conformation on Ti. In general, the conformation of proteins on metals is influenced by the relative permittivity, which is dependent on the metal oxide. The relative permittivity in TiO_2 was larger than those in other metal oxides and close to that of H_2O. Sundgren et al.[41] reported that the conformation change of fibrinogen was more extensive on Au than on Ti. When the conformational flexibility of proteins is low, they might be more easily detached. In the case of electrodeposited specimens, bacteria and WIG are directly adsorbed onto Ti surfaces because protein adsorption was inhibited. Therefore, the binding force between the Ti surface and biofilm is expected to be very weak, resulting in biofilms on PEG-Ti detaching relatively easily. Hence, the null hypothesis seems to be proven correct in this study, suggesting that controlling protein adsorption at the initial stage of biofilm formation is potentially useful as a strategy for the inhibition of biofilm formation.

CONCLUSIONS

We evaluated PEG-Ti surfaces using an OBR to determine whether the surface was effective for the inhibition of bacterial adhesion and biofilm formation. The attachment of *S. gordonii* was inhibited on the PEG-Ti surfaces resulting from the stabilization of PEGs and neutralization of surface charges. Furthermore, *S. mutans* biofilms were easier to detach from the surface of PEG-Ti. Moreover, the PEG-Ti surface inhibited salivary protein adsorption. In addition, it was determined that electrodeposited PEG was more effective on rough surface rather than on smooth surfaces. The degree of the detachment of biofilms from PEG-Ti indicated an association with the inhibition of the salivary protein adsorption, suggesting weak basal attachment of the biofilms. Therefore, controlling protein adsorption at an initial stage may be an effective strategy to protect the metal surfaces from biofilm formation.

ACKNOWLEDGMENTS

The authors thank Prof. Howard H. Kuramitsu, State University of New York at Buffalo, for his kind contribution in editing the manuscript.

REFERENCES

1. Dibart S, Warbington M, Su MF, Skobe Z. In vitro evaluation of the implant-abutment bacterial seal: The locking taper system. Int J Oral Maxillofac Implant 2005;20:732–737.
2. Glauser R, Schupbach P, Gottlow J, Hammerle CHF. Periimplant soft tissue barrier at experimental one-piece mini-implants with different surface topography in humans: A light-microscopic overview and histometric analysis. Clin Implant Dent Relat Res 2005;7: S44–S51.
3. Tesmer M, Wallet S, Koutouzis T, Lundgren T. Bacterial colonization of the dental implant fixture-abutment interface: An in vitro study. J Periodontol 2009;80:1991–1997.
4. MacKintosh EE, Patel JD, Marchant RE, Anderson JM. Effects of biomaterial surface chemistry on the adhesion and biofilm formation of Staphylococcus epidermidis *in vitro*. J Biomed Mater Res A 2006;78:836–842.
5. Sendi P, Rohrbach M, Graber P, Frei R, Ochsner PE, Zimmerli W. *Staphylococcus aureus* small colony variants in prosthetic joint infection. Clin Infect Dis 2006;43:961–967.
6. Barberan J, Aguilar L, Gimenez MJ, Carroquino G, Granizo JJ, Prieto J. Levofloxacin plus rifampicin conservative treatment of 25 early staphylococcal infections of osteosynthetic devices for rigid internal fixation. Int J Antimicrob Agent 2008;32:154–157.
7. Cramton SE, Gerke C, Schnell NF, Nichols WW, Götz F. The intercellular adhesion (*ica*) locus is present in *Staphylococcus aureus* and is required for biofilm formation. Infect Immun 1999;67: 5427–5433.
8. Hamada S, Slade HD. Biology, immunology, and cariogenicity of *Streptococcus mutans*. Microbiol Rev 1980;44:331–384.
9. Ooshima T, Matsumura M, Hoshino T, Kawabata S, Sobue S, Fujiwara T. Contributions of three glucosyltransferases to sucrose-dependent adherence of *Streptococcus mutans*.. J Dent Res 2001;80: 1672–1677.
10. Ono M, Nikaido T, Ikeda M, Imai S, Hanada N, Tagami J, Matin K. Surface properties of resin composite materials relative to biofilm formation. Dent Mater J 2007;26:613–622.
11. Meredith DO, Eschbach L, Wood MA, Riehle MO, Curtis ASG, Richards RG. Human fibroblast reactions to standard and electropolished titanium and Ti-6Al-7Nb, and electropolished stainless steel. J Biomed Mater Res A 2005;75:541–555.
12. Koerner RJ, Butterworth LA, Mayer IV, Dasbach R, Busscher HJ. Bacterial adhesion to titanium-oxy-nitride (TiNOX) coatings with different resistivities: A novel approach for the development of biomaterials. Biomaterials 2002;23:2835–2840.
13. Simonetti N, Simonetti G, Bougnol F, Scalzo M. Electrochemical Ag^+ for preservative use. Appl Environ Microbiol 1992;58: 3834–3836.
14. Wassall MA, Santin M, Isalberti C, Cannas M, Denyer SP. Adhesion of bacteria to stainless steel and silver-coated orthopedic external fixation pins. J Biomed Mater Res A 1997;36:325–330.
15. Massè A, Bruno A, Bosetti M, Biasibetti A, Cannas M, Gallinaro P. Prevention of pin track infection in external fixation with silver coated pins: Clinical and microbiological results. J Biomed Mater Res B Appl Biomater 2000;53:600–604.
16. Alt V, Bechert T, Steinrücke P, Wagener M, Seidel P, Dingeldein E, Domann E, Schnettler R. An in vitro assessment of the antibacterial properties and cytotoxicity of nanoparticulate silver bone cement. Biomaterials 2004;25:4383–4391.
17. Kraft CN, Hansis M, Arens S, Menger MD, Vollmar B. Striated muscle microvascular response to silver implants: A comparative in vivo study with titanium and stainless steel. J Biomed Mater Res A 1999;49:192–199.
18. Harris LG, Tosatti S, Wieland M, Textor M, Richards RG. *Staphylococcus aureus* adhesion to titanium oxide surfaces coated with non-functionalized and peptide-functionalized poly(L-lysine)-*grafted*-poly(ethylene glycol) copolymers. Biomaterials 2004;25: 4135–4148.
19. Tanaka Y, Doi H, Iwasaki Y, Hiromoto S, Yoneyama T, Asami K, Imai H, Hanawa T. Electrodeposition of amine-terminated poly(ethylene glycol) to titanium surface. Mater Sci Eng C 2007;27: 206–212.
20. Tanaka Y, Matsuo Y, Komiya T, Tsutsumi Y, Doi H, Yoneyama T, Hanawa T. Characterization of the spatial immobilization manner of poly(ethylene glycol) to a titanium surface with immersion and electrodeposition and its effects on platelet adhesion. J Biomed Mater Res A 2010;92:350–358.
21. Okada A, Nikaido T, Ikeda M, Okada K, Yamauchi J, Sawada H, Tagami J, Matin K. Inhibition of biofilm formation using newly developed coating materials with self-cleaning properties. Dent Mater J 2008;27:565–572.

22. Gyo M, Nikaido T, Okada K, Yamauchi J, Tagami J, Matin K. Surface response of fluorine polymer-incorporated resin composites to cariogenic biofilm adherence. Appl Environ Microbiol 2008;74: 1428–1435.
23. Asami K. A precisely consistent energy calibration method for X-ray photoelectron spectroscopy. J Electron Spectrosc 1976;9: 469–478.
24. Shirley DA. High-resolution X-ray photoemission spectrum of the valence bands of gold. Phys Rev 1972;B5:4709–4714.
25. Ashwell G. The phenol-sulfuric acid reaction for carbohydrates. Methods Enzymol 1966;8:93–95.
26. Tanaka Y, Doi H, Kobayashi E, Yoneyama T, Hanawa T. Determination of the immobilization manner of amine-terminated poly (ethylene glycol) electrodeposited on a titanium surface with XPS and GD-OES. Mater Trans 2007;28:287–292.
27. Tanaka Y, Saito H, Tsutsumi Y, Doi H, Imai H, Hanawa T. Active hydroxyl groups on surface oxide film of titanium, 316L stainless steel, and cobalt-chromium-molybdenum alloy and its effect on the immobilization of poly(ethylene glycol). Mater Trans 2008;49: 805–811.
28. Oya K, Tanaka Y, Saito H, Kurashima K, Nogi K, Tsutsumi H, Tsutsumi Y, Doi H, Nomura N, Hanawa T. Calcification by MC3T3-E1 cells on RGD peptide immobilized on titanium through electrodeposited PEG. Biomaterials 2009;30:1281–1286.
29. Tanaka Y, Saito H, Tsutsumi Y, Doi H, Nomura N, Imai H, Hanawa T. Effect of pH on the interaction between zwitterions and titanium oxide. J Colloid Interface Sci 2009;330:138–143.
30. Kolenbrander PE, Andersen RN, Blehert DS, Egland PG, Foster JS, Palmer RJ Jr. Communication among oral bacteria. Microbiol Mol Biol Rev 2002;66:486–505.
31. Jeon SI, Lee JH, Andradea JD, De Gennes PG. Protein-surface interactions in the presence of polyethylene oxide I. Simplified theory. J Colloid Interface Sci 1991;142:149–166.
32. Claesson P. Poly(ethylene oxide) surface coatings: Relations between intermolecular forces, layer structure and protein repellency. Colloid Surf A 1983;77:109–118.
33. Rogers JD, Palmer RJ Jr, Kolenbrander PE, Scannapieco FA. Role of *Streptococcus gordonii* amylase-binding protein A in adhesion to hydroxyapatite, starch metabolism, and biofilm formation. Infect Immun 2001;69:7046–7056.
34. Hajishengallis G, Koga T, Russell MW. Affinity and specificity of the interactions between *Streptococcus mutans* antigen I/II and salivary components. J Dent Res 1994;73:1493–1502.
35. Delmi M, Vaudaux P, Lew DP, Vasey H. Role of fibronectin in staphylococcal adhesion to metallic surfaces used as models of orthopaedic devices. J Orthop Res 1994;12:432–438.
36. Ha KY, Chung YG, Ryoo S. Adherence and biofilm formation of *Staphylococcus epidermidis* and *Mycobacterium tuberculosis* on various spinal implants. J Spine 2005;30:38–43.
37. Gracia E, Fernández A, Conchello P, Laclériga A, Paniagua L, Seral F, Amorena B. Adherence of *Staphylococcus aureus* slime-producing strain variants to biomaterials used in orthopaedic surgery. Int Orthop 1997;21:46–51.
38. Tanner J, Robinson C, Söderling E, Vallittu P. Early plaque formation on fibre-reinforced composites in vivo. Clin Oral Investig 2005;9:154–160.
39. Amano A, Sharma A, Lee JY, Sojar HT, Raj PA, Genco RJ. Structural domains of *Porphyromonas gingivalis* recombinant fimbrillin that mediate binding to salivary proline-rich protein and statherin. Infect Immun 1996;64:1631–1637.
40. Petersen FC, Assev S, van der Mei HC, Busscher HJ, Scheie AA. Functional variation of the antigen I/II surface protein in *Streptococcus mutans* and *Streptococcus intermedius*. Infect Immun 2002;70:249–256.
41. Sundgren J-E, Bodö P, Ivarsson B, Lundström I. Adsorption of fibrinogen on titanium and gold surface studied by ESCA and ellipsometry. J Colloid Interface Sci 1986;113:530–543.

2664 *Macromolecules* **2010**, *43*, 2664–2666
DOI: 10.1021/ma100242s

Macromolecules
COMMUNICATION TO THE EDITOR

Synthesis of Well-Defined Thermoresponsive Polyphosphoester Macroinitiators Using Organocatalysts

Yasuhiko Iwasaki* and Etsuko Yamaguchi

Department of Chemistry and Materials Engineering, Faculty of Chemistry, Materials and Bioengineering, Kansai University, 3-3-35 Yamate-cho, Suita-shi, Osaka 564-8680, Japan

Received February 1, 2010
Revised Manuscript Received February 19, 2010

Polyphosphoesters have a high impact in bio-related fields because of their biocompatibility and structural similarities to naturally occurring nucleic acids.[1−3] The phosphoester backbone is degradable through spontaneous hydrolysis; the degradation is accelerated with enzymatic treatment.[4] A variety of synthetic routes for polyphosphoesters have been proposed, including ring-opening polymerization (ROP),[5−7] polycondensation,[8] transesterification,[9,10] and enzymatic polymerization.[11] Although there have been a few reports of synthesizing high molecular weight polyphosphoesters,[12,13] there have been limitations on obtaining high molecular weight with narrow distribution. For reliable properties and advanced applications of polymers, the exploration of novel synthetic processes is needed.

The ROP of cyclic phosphoesters is the most common process used to obtain polyphosphoesters. This is because a variety of polyphosphoesters can be designed in comparison with conventional biodegradable polymers because cyclic phosphoesters are obtained as monomers from the condensation of alcohol and 2-chloro-2-oxo-1,3,2-dioxaphospholane.[14] Using some alcohol compounds, biodegradable macro-cross-linkers[4] and macroinitiators for atom transfer radical polymerization (ATRP)[15] have already been prepared. These polyphosphoesters are building blocks for constructing novel polymer materials.

For the ROP of cyclic phosphoesters, metallic compounds are commonly used as initiators or polymerization catalysts.[5−7,16] Although the polymerization processes are very successful in producing polyphosphoesters, the metal compounds are environmentally sensitive, and a lack of residual metal contaminants is required in biomedical applications. Recently, organocatalysts have been the focus of the modern synthetic processes of polyesters, polycarbonates, and silicones.[17] One of the most successful procedures for making biodegradable polymers is polymerization using guanidine and amidine bases both in bulk and in solution. Nederberg and Hedrick prepared poly(trimethylene carbonate (TMC)) (PTMC) with the base catalysts in the presence of benzyl alcohol.[18] Excellent controlled polymerization conditions were performed with several catalysts, and PTMCs with relatively high molecular weight, narrow distribution, and high yield were obtained. Although organocatalysts have high potency for ROP, they have not been used for the polymerization of cyclic phosphoesters. We report here the first ROP of cyclic phosphoesters using 1,8-diazabicyclo[5.4.0]undec-7-ene (DBU) or 1,5,7-triazabicyclo[4.4.0]dec-5-ene (TBD) as an organocatalyst. Compared with polymerization using metallic catalysts, control of the polymerization of cyclic phosphoesters was much less difficult.

*Corresponding author: Fax +81-6-6368-0090; Tel +81-6-6368-0090; e-mail yasu.bmt@kansai-u.ac.jp.

The synthetic routes of poly(2-isopropoxy-2-oxo-1,3,2-dioxaphospholane) (PIPP) and its block copolymer are shown in Scheme 1. According to the new synthetic process, we have succeeded in synthesizing well-defined polyphosphoesters with both a narrow molecular weight distribution and a high molecular weight. Furthermore, block copolymers with 2-methacryloyloxyethylphosphorylcholine (MPC) were synthesized by using PIPP as a macroinitiator. Such well-defined polymer synthesis may be important for obtaining biomimetic and reliable functions because a biopolymer always has an exact molecular weight without any distribution.

IPP and HEBB were synthesized by the previously described method.[15] PIPP was synthesized by ROP using an organocatalyst as an initiator in the presence of HEBB (Scheme 1). In the case of DBU, polymerization was homogeneously performed in a solvent-free condition. In contrast, a small amount of toluene was used for dissolving TBD to make a homogeneous solution. The results of PIPP synthesis are summarized in Table 1. 20 mmol of IPP was first introduced into a polymerization tube under an argon gas atmosphere at 0 °C, and then a given amount of HEBB was added to the tube. Finally, a given amount of organocatalyst was introduced. Polymerization was carried out at 0 °C. The range of molecular weights was approximately 2.0×10^3–3.0×10^4 g/mol by a JASCO gel-permeation chromatography (GPC) system using a calibration curve based on linear polystyrene standards with chloroform as the mobile phase. In every case, the molecular weight distribution was lower than 1.10. Under each condition, the molecular weights of the synthetic polymers agreed with the theoretical values.

Figure 1 shows the M_n versus monomer conversion for the polymerization of IPP by using DBU as a catalyst. The plot of the number-averaged molecular weight (M_n) vs conversion was linear up to 60% conversion. The linearity of the plot suggested that the number of macromolecules in the reaction system was constant during polymerization. The molecular weight distribution of PIPP was narrow and stable during polymerization. The mechanism of ROP with organocatalysts was characterized using ^{1}H NMR by Hedrick and co-workers.[18,19] They indicated that DBU and TBD form hydrogen bonds to the alcohol of an initiator. ROP of IPP with DBU then occurred through a quasi-anionic polymerization mechanism by activation of the alcohol of the initiator. In contrast, the increase in the monomer conversion for the polymerization of IPP between DBU and TBD was significantly different. When TBD was used as a catalyst, the conversion of PIPP reached a level of more than 75% within 20 min. The heightened activity of TBD for the polymerization of lactone and TMC was also observed.[18] TBD has two activation sites in the molecule and is capable of an acyl transfer reaction. From a ^{1}H NMR study, a remarkable shift of the alcohol proton of HEBB at 3.86 ppm was observed in a toluene-d_8 solution containing HEBB and TBD (1:1, 0.05 M); that is, TBD has a hydrogen bond acceptor for the hydroxylic proton of HEBB (see Supporting Information Figure S1). Because the N−H site of the TBD might activate IPP, a ^{1}H NMR analysis of the mixture of TBD and IPP (1:5, 0.05 M) was carried out. The spectra are summarized in Figure 2.

The dashed symbols in Figure 2 represent the shifted signals of the protons of IPP. Although the signal of the original cyclic IPP remained in the solution, ring-opening IPP was also observed. According to previous literature describing ROP of TMC or L-lactide with TBD,[18,19] we assumed that TBD served as a dual activation catalyst for the cyclic phosphoester and initiator. The

 Published on Web 02/26/2010

Table 1. Synthetic Results of PIPP

code	catalyst	$[M]_0/[I]$	HEBB (mmol)	catalyst (mmol)	time (min)	conversion (%)	$M_n \times 10^{-3}$	M_w/M_n	$M_{n(Theo)} \times 10^{-3}$
$PIPP_{13}$	DBU	25	0.80	1.20	60	52.8	2.4	1.03	2.2
$PIPP_{32}$	DBU	50	0.40	0.60	90	52.7	4.7	1.07	4.4
$PIPP_{50}$	DBU	100	0.20	0.30	300	50.8	7.7	1.09	8.4
$PIPP_{48}$	TBD	50	0.40	0.20	20	81.2	8.2	1.06	6.7
$PIPP_{77}$	TBD	100	0.20	0.20	20	80.7	13.0	1.09	13.4
$PIPP_{117}$	TBD	150	0.13	0.20	20	75.5	16.9	1.07	18.8
$PIPP_{174}$	TBD	200	0.10	0.20	20	90.3	28.9	1.05	30.0

Scheme 1. Synthetic Routes of Poly(2-isopropoxy-2-oxo-1,3,2-dioxaphospholane) (PIPP) and Poly(2-methacryloyloxyethylphosphorylcholine-*b*-PIPP)

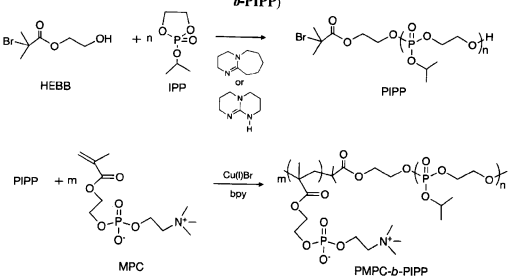

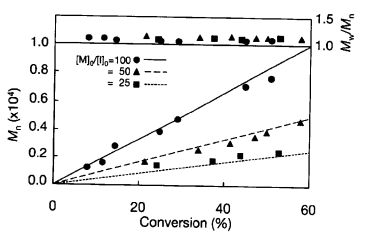

Figure 1. Plot of M_w/M_n and M_n versus monomer conversion for the polymerization of 2-isopropoxy-2-oxo-1,3,2-dioxaphospholane by using 1,8-diazabicyclo[5.4.0]undec-7-ene as a catalyst. Broken lines suggest the theoretical amount of each polymerization condition.

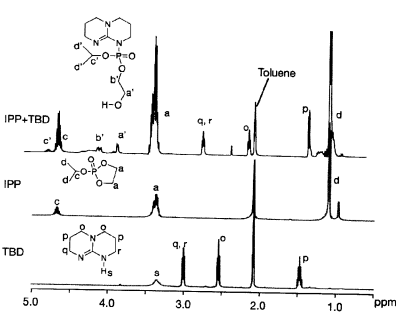

Figure 2. ^1H NMR spectra of 1,5,7-triazabicyclo[4.4.0]dec-5-ene (TBD), 2-isopropoxy-2-oxo-1,3,2-dioxaphospholane (IPP), and their mixture in toluene-d_8. Dashed symbols represent the intermolecular interaction of TBD and IPP in the solution.

N−H site of TBD served as a hydrogen bond donor and might interact with the oxygen of the five-membered ring of IPP. A nucleophilic attack of the imine nitrogen on the phosphorus would then generate TBD aminophosphonate, as shown in Figure 2, following hydrogen-bond activation of the HEBB alcohol, which should facilitate the formation of phosphoester and regeneration of TBD. As expected, every ^1H NMR signal was caused by each molecule in the mixture of DBU and IPP (1:1, 0.05 M), and no signals were caused by intermolecular interactions (see Supporting Information Figure S2). DBU only activated HEBB.

The glass transition temperature (T_g) of $PIPP_{77}$, which was determined by differential scanning calorimetry, was −52.7 °C, and that of the highly viscous polymers, summarized in Table 1, was room temperature.

We have recently discovered that aqueous solutions containing polyphosphoesters bearing simple alkyl chains showed LCST-type phase separation behavior.[20,21] The phase separation temperature of polyphosphoesters is influenced by the chemical structure of the side chain and able to control its polarity. Very recently, we synthesized polyphosphoesters bearing enzymatic cleavable chains.[21] The phase separation temperature increased with an increase in the incubation time of the enzyme. Wang and co-workers also observed the thermoresponsivity of polyphosphoesters. They have synthesized well-defined block copolymers of poly(ethylene glycol) and polyphosphoester.[22] The block copolymers can form core−shell type polymeric micelles in an aqueous medium with the effect of temperature caused by self-association of the polyphosphoester block. Although it is clear that polyphosphoester is the new candidate thermoresponsive polymer, its properties have only been partially evaluated. The effect of molecular weight on the cloud point of PIPP has not been discussed. Figure 3 shows the molecular weight dependence of the phase separation temperature of PIPP in phosphate buffered saline (PBS).

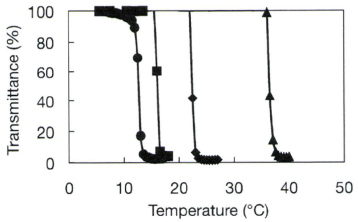

Figure 3. Effect of molecular weight on cloud point of poly(2-isopropoxy-2-oxo-1,3,2-dioxaphospholane) (PIPP) (1 wt %) in PBS: (●) $PIPP_{50(DBU)}$, (■) $PIPP_{48(TBD)}$, (◆) $PIPP_{32(DBU)}$, (▲) $PIPP_{13(DBU)}$.

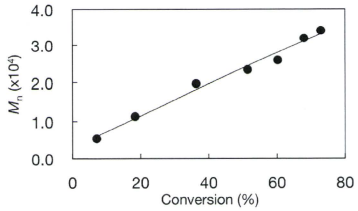

Figure 4. Plot of M_n versus monomer conversion for polymerization of 2-methacryloyloxyethylphosphorylcholine by using a macroinitiator ($PIPP_{77}$).

The cloud point of the polymer solution linearly decreases with an increase in the molecular weight of PIPP. This result indicates that the type of organocatalyst does not influence the phase separation temperature. The phase separation temperature of polyphosphoesters is influenced by the chemical structure of the side chains, the concentration, and the ion strength of the aqueous media.[21] In our previous report, PIPP that was synthesized using triisobutylaluminum as an initiator was not soluble in water even when the molecular weight was less than 1.0×10^4.[15] An uncontrolled reaction might occur when a metallic catalyst was used. Wang reported that long-term polymerization of cyclic phosphoesters with $Sn(Oct)_2$ makes some branch structures with high conversion.[16] In addition, some side reactions might occur in ring-opening polymerization of five-membered cyclic phosphoesters at high temperature.[23] Furthermore, the molecular weight distribution of polyphosphoesters synthesized with an organocatalyst was significantly narrow compared with polymers that used metallic catalysts. The advantages of using organocatalysts can be observed on the synthesis of well-defined polymers with high conversion.

Using $PIPP_{77}$ as a macroinitiator, we synthesized well-defined, biocompatible block copolymers with 2-methacryloyloxyethylphosphorylcholine (MPC)[24] in the presence of copper(I) bromide and 2,2′-bipyridine (bpy), as shown in Scheme 1. M_n and molecular weight distribution of $PIPP_{77}$-*b*-PMPC were measured with a JASCO GPC system with a refractive index detector and size-exclusion columns, using poly(ethylene glycol) (PEG) standard in distilled water containing 10 mM LiBr. The concentration of polymer solution for this measurement was adjusted to below 0.01 wt % to reduce polymer association. Figure 4 shows the dependence, M_n, on conversion for ATRP of MPC from the end of PIPP. The plot of M_n versus monomer concentration was linear up to 80% conversion. The linearity of the plot suggests that the number of polymer molecules remained constant and that polymerization could be controlled on a polymerization time scale. The molecular weight distribution (M_w/M_n) was below 1.5. Although the intermolecular interaction of the block copolymer was too weak to obtain stable polymer associates at this point, it was demonstrated that well-defined block copolymers with narrow molecular weight distributions could be obtained. Recently, it has been also reported that zwitterionic phosphorylcholine showed better stabilization than did PEG.[25] By controlling the structure of the side chains of PIPP to enhance molecular interaction, novel biocompatible nanomaterials might be obtained.

In summary, this study explored a modern synthetic route of polyphosphoesters with the use of organocatalysts. For this synthetic process, various types of alcohols can be used as initiators; that is, the end functionalities of the block copolymers can be controlled.

Acknowledgment. This work was supported by a Grant-in-Aid for Young Scientists (A) from the Ministry of Education, Culture, Sports, Science and Technology of Japan (#21680043).

Supporting Information Available: Experimental method and ^1H NMR spectra representing interactions between organocatalysts and initiators or monomers. This material is available free of charge via the Internet at http://pubs.acs.org.

References and Notes

(1) Penczek, S.; Pretula, J.; Kaluzynski, K. *Biomacromolecules* **2005**, *6*, 547–551.
(2) Zhao, Z.; Wang, J.; Mao, H. Q.; Leong, K. W. *Adv. Drug Delivery Rev.* **2003**, *55*, 483–499.
(3) Wang, Y.-C.; Yuan, Y.-Y.; Du, J.-Z.; Yang, X.-Z.; Wang, J. *Macromol. Biosci.* **2009**, *9*, 1154–1164.
(4) Wachiralarpphaithoon, C.; Iwasaki, Y.; Akiyoshi, K. *Biomaterials* **2007**, *28*, 984–993.
(5) Penczek, S.; Klosinski, P. In *Model of Biopolymer by Ring-Opening Polymerization*; Penczek, S. Ed.; CRC Press: Boca Raton, FL, 1990; p 291.
(6) Libiszowski, J.; Kaluzynski, K.; Penczek, S. *J. Polym. Sci., Part A: Polym. Chem.* **1978**, *16*, 1275–1283.
(7) Pretula, J.; Kaluzynski, K.; Penczek, S. *Macromolecules* **1986**, *19*, 1797–1799.
(8) Richards, M.; Dahiyat, B. I.; Arm, D. M.; Lin, S.; Leong, K. W. *J. Polym. Sci., Part A: Polym. Chem.* **1991**, *29*, 1157–1165.
(9) Pretura, J.; Kaluzynski, K.; Szymanski, R.; Penczek, S. *J. Polym. Sci., Part A: Polym. Chem.* **1999**, *37*, 1365–1381.
(10) Myrex, R. D.; Farmer, B.; Gray, G. M.; Wright, Y.-J.; Dees, J.; Bharara, P. C.; Byrd, H.; Branham, K. E. *Eur. Polym. J.* **2003**, *39*, 1105–1115.
(11) Wen, J.; Zhuo, R. X. *Macromol. Rapid Commun.* **1998**, *19*, 641–642.
(12) Kaluiyhski, K.; Libiszowski, J.; Penczek, S. *Makromol. Chem.* **1977**, *178*, 2943–2947.
(13) Katuiyhski, K.; Libiszowski, J.; Penczek, S. *Macromolecules* **1976**, *9*, 365–367.
(14) Edmundson, R. S. *Chem. Ind. (London)* **1962**, 1828.
(15) Iwasaki, Y.; Akiyoshi, K. *Macromolecules* **2004**, *37*, 7637–7642.
(16) Xiao, C.-S.; Wang, Y.-C.; Du, J.-Z.; Chen, X.-S.; Wang, J. *Macromolecules* **2006**, *39*, 6825.
(17) Kamber, N. E.; Jeong, W.; Waymouth, R. M.; Pratt, R. C.; Lohmeijer, B. G. G.; Hedrick, J. L. *Chem. Rev.* **2007**, *107*, 5813–5840.
(18) Nederberg, F.; Lohmeijer, B. G. G.; Leibfarth, F.; Pratt, R. C.; Choi, J.; Dove, A. P.; Waymouth, R. M.; Hedrick, J. L. *Biomacromolecules* **2007**, *8*, 153–160.
(19) Pratt, R. C.; Lohmeijer, B. G. G.; Long, D. A.; Waymouth, R. M.; Hedrick, J. L. *J. Am. Chem. Soc.* **2006**, *128*, 4556–4557.
(20) Iwasaki, Y.; Wachiralarpphaithoon, C.; Akiyoshi, K. *Macromolecules* **2007**, *40*, 8136–8138.
(21) Iwasaki, Y.; Kawakita, T.; Yusa, S. *Chem. Lett.* **2009**, *38*, 1054–1055.
(22) Wang, Y. C.; Tang, L. Y.; Li, Y.; Wang, J. *Biomacromolecules* **2009**, *10*, 66–73.
(23) Liu, J.; Huang, W.; Zhou, Y.; Yan, D. *Macromolecules* **2009**, *42*, 4394–4399.
(24) Iwasaki, Y.; Ishihara, K. *Anal. Bioanal. Chem.* **2005**, *381*, 534–546.
(25) Jin, Q.; Xu, J. P.; Ji, J.; Shen, J. C. *Chem. Commun.* **2008**, 3058–3060.

J Mater Sci (2010) 45:1796–1802
DOI 10.1007/s10853-009-4161-9

Compressive creep behavior of silane treated TiO_2/high-density polyethylene

C. X. Dong · S. J. Zhu · M. Mizuno · M. Hashimoto

Received: 25 October 2009 / Accepted: 21 December 2009 / Published online: 5 January 2010

Abstract In biomaterial silane treated TiO_2/high-density polyethylene(silane–TiO_2/HDPE), silane connection structurally corresponds to acid phosphoprotein bond, which connects the noncalcified collagen fibril bands and the adjacent apatite crystals in natural bones. In order to explore the function and variation process of acid phosphoprotein under loading in natural bones, the microscopic variation mechanism of silane connection in silane–TiO_2/HDPE was investigated through the compressive creep tests in air and saline solution. Through the analysis of creep rate curves under different stress loads, different creep mechanisms were proposed, in which silane connection plays a very important role. Through SEM observation of sample surfaces and the creep tests in saline solution, the important role of silane connection in creep process was further proved. That is, silane connection can not only support the loading stress but also hinder the failure process under loading effectively.

Introduction

Designing an ideal bone graft that emulates natural bone's own structure is the common design strategy for bone biomaterial development. It is well known that natural bones mainly consist of noncalcified collagen fibril bands and the adjacent apatite crystals, between which acid phosphoprotein bonds connect them. Therefore, the composites of inorganic fillers and organic matrix sound a good choice for the design of bone biomaterials.

Based on this idea, a composite of hydroxyapatite particles with high-density polyethylene (HAPEX) was developed by Bonfield in the early 1980s [1]. However, the fracture toughness and elastic modulus of HAPEX are lower than those of heavy load bearing bones. Compared with hydroxyapatite, TiO_2 has higher elastic modulus, so Kokubo et al. [2] developed biomaterial of TiO_2/HDPE with high bioactivity. The bending strength and Young's modulus were found to vary from almost 28 to 54 MPa and 1.4 to 7.6 GPa, respectively, depending on the TiO_2 content. To improve weak mechanical adhesion at interfaces effectively, a silane coupling agent was used to modify the surface of TiO_2 particles [3]. The silane coupling agent connects TiO_2 and HDPE by formation of chemical bonds at both of its ends, which can improve the mechanical properties greatly. It should be noted that the silane connection between TiO_2 and HDPE structurally corresponds to acid phosphoprotein bonds in natural bones.

The mechanical behavior of bone tissue's ultra- and micro-structure is fundamental to assess macroscopic bone mechanics. It is also true for biomaterials. Ascenzi et al. made their hypothesis that the acid phosphoprotein bonds between the noncalcified collagen fibril bands and the adjacent apatite crystals tend to weaken and eventually break under mechanical loading [4]. However, this hypothesis has not been proved by other research work. Furthermore, whether the corresponding microstructure in synthesized biomaterials experiences the same process is also meaningful problem.

C. X. Dong · S. J. Zhu (✉)
Department of Intelligent Mechanical Engineering, Fukuoka Institute of Technology, Fukuoka 811-0295, Japan
e-mail: zhu@fit.ac.jp

C. X. Dong
College of Chemistry and Biology, Beihua University, Jilin City 132013, China

M. Mizuno · M. Hashimoto
Japan Fine Ceramics Center, Nagoya 456-8587, Japan

For polymer composites, creep behavior is very important for practical application. There are some reports on the creep behaviors of polymer composites filled with inorganic particles [5–7]. For example, Yang et al. [8] carried out tensile creep tests on a few polyamide 66 composites filled with different nanoparticles. One of them was a composite with 1 wt% 21 nm TiO_2 particles modified with octylsilane. It was found that the creep resistance of nanocomposites was significantly enhanced by nanoparticles without sacrificing the tensile properties. Lietz et al. [9] investigated the mechanical properties and creep resistance of SBS block copolymers with nanoclay fillers and found that the introduction of dispersed nanoclays induced promising improvements in creep performance. Although surface modifications of nanofillers with organic chemicals are widely used [10–13], the effect of chemical connection between inorganic particle and organic matrix on creep behaviors was seldom found.

In this work, the microscopic variation mechanism of silane connection in silane–TiO_2/HDPE was investigated through compressive creep tests. Through the analysis of creep rate curves, the creep mechanisms were proposed, in which silane connection plays a key role. That is, upon loading silane connection supports load, stretches to relieve load and is finally broken by the concentrated stress.

Experimental procedures

Materials

Silane treated TiO_2/high-density polyethylene (silane–TiO_2/HDPE) composite was fabricated in Japan Fine Ceramics Center. The ratio of TiO_2 to HDPE is 40vol.%, with anatase mean particle size of 535 nm. TiO_2 powder was treated with silane-coupling agent of γ-MPS (γ[-(methacryloxy)propyl]trimethoxysilane) and mixed with HDPE. During the manufacturing process, kneading and compression molding was involved. The detailed manufacturing process was described in literature [3]. By the analysis of FTIR, it was confirmed that the surface of TiO_2 particles was connected with HDPE through formation of Ti–O–Si bonds.

Compressive creep

The specimens of silane–TiO_2/HDPE were cut to cylindrical shape and polished to diameter of 6 mm and height of 12 mm. A servo-hydraulic fatigue machine Model EHF-EB5 (Shimadzu Co. Ltd., Japan) was employed to carry out the tests. In compressive strength tests, the rate of displacement was maintained at 0.033 mm/s. Tests were carried out in air or in saline solution of 0.9% NaCl. The temperature was kept to be 25 °C in the two conditions. The temperature controlling of saline solution was realized by pumping and recycling the saline solution of 25 °C into the test trough during test process.

Morphology observation

For the tested samples, it is somewhat difficult to observe the fracture surfaces because friction of them during compressive process has blurred the fracture information. For explanation of the possible fracture mechanism, the outer side surfaces of tested specimens were observed by scanning electronic microscopy (SEM) Hitachi S-3000N. Prior to observation, the samples were cleaned ultrasonically and dried. Then the outer side surfaces were coated with Au to ensure clear images using Hitachi ion sputter E-1010. The layer thickness of Au coating is about 10 nm.

Results and discussion

Compressive properties

Compressive tests were performed in air and saline solution at room temperature for silane–TiO_2/HDPE. The compressive curves are shown in Fig. 1. The Young's moduli are 2.9 GPa in air and 2.1 GPa in saline solution. Compressive strengths are 71 MPa in air and 63 MPa in saline solution. Obviously, silane–TiO_2/HDPE is susceptible to saline solution, which resulted in lower Young's modulus and compressive strength.

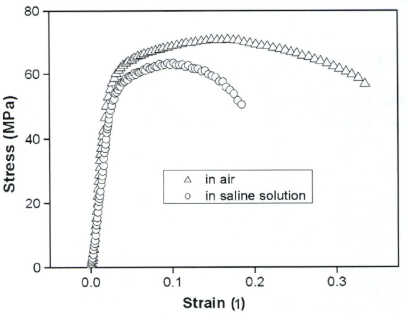

Fig. 1 Compressive stress–strain curves of silane–TiO_2/HDPE at room temperature in different surrounding conditions